Journal of Applied Electrochemistry (2005) 35:857–864
DOI 10.1007/s10800-005-2572-0

Synthetic diamond electrodes: The effect of surface microroughness on the electrochemical properties of CVD diamond thin films on titanium

YU. V. PLESKOV[1,*], YU. E. EVSTEFEEVA[1], M.D. KROTOVA[1], P.Y. LIM[2,3], H.C. SHIH[3], V.P. VARNIN[4], I.G. TEREMETSKAYA[4], I.I. VLASOV[5] and V.G. RALCHENKO[5]
[1]*Frumkin Institute of Electrochemistry, Russian Academy of Sciences, Leninskii prosp. 31, Moscow 119071, Russia*
[2]*Industrial Technology Research Institute, Bldg. 77, 195 Chung Hsing Rd. Sec. 4 Chutung Hsinchu, Taiwan310, R.O.C.*
[3]*Department of Materials Science and Engineering, National Tsing Hua University, 101 Sec. 2, Kuang Fu Road Hsinchu Taiwan300, R.O.C.*
[4]*Institute of Physical Chemistry, Russian Academy of Sciences, Leninskii prosp. 31, Moscow 117915, Russia*
[5]*General Physics Institute, Russian Academy of Sciences, Vavilov str. 38 Moscow 119991, Russia*
*(*author for correspondence, e-mail: pleskov@electrochem.msk.ru)*

Received 6 July 2004; accepted in revised form 7 February 2005

Key words: diamond, electrochemical kinetics, microroughness, thin-film electrode, titanium substrate

Abstract

The electrochemical behavior of B-doped diamond films on Ti substrates subjected to different pretreatment procedures (annealing, sand-blasting, and etching in HCl) is evaluated as a function of surface microroughness. Generally, the differential capacitance follows the true surface area of the electrodes. The width of the potential window also increases, but slightly, with the roughness. The electrode reversibility in the $[Fe(CN)_6]^{3-}/[Fe(CN)_6]^{4-}$ redox system increases with increasing surface roughness. The apparent increase in the reversibility of the reaction may be also explained by the decrease in the true current density. Although the variations in the electrochemical parameters are not strongly pronounced, the tendencies observed can be used to optimise the electrode properties.

1. Introduction

Interest in synthetic diamond electrodes in fundamental and applied electrochemistry is widening [1, 2]. Comprehensive evaluation of polycrystalline diamond electrodes requires knowledge of the effects of surface structure on the electrochemical behavior of diamond. Numerous papers have dealt with the effects of intercrystallite boundaries [3], single crystal face orientation [4, 5], grain size [6] (including nanodiamond films [7, 8]), nanostructured (''nano-honeycomb'') surface relief [9, 10] and sp^2 -carbon inclusions [11, 12], on the electrochemical properties of diamond electrodes. However, no studies on the dependence of diamond electrode behavior on its surface roughness have been performed, to our knowledge.

This work presents a comparative study of CVD-diamond thin-film electrodes with varying surface roughness. To this purpose, we deposited boron-doped diamond (BDD) films on titanium substrates subjected to different pretreatment procedures (annealing, sand-blasting and etching), thus producing roughened surfaces. Titanium seems to be a promising substrate material due to compromise between material cost, mechanical stability, corrosion resistance and diamond coating adherence. Currently large-area, up to 0.5 m^2, diamond electrodes on Ti are produced commercially, in particular for wastewater treatment [13, 14]. The details of Ti substrate preparation for producing high-quality diamond films are discussed in [15, 16].

The deposited films were characterized by various methods, including surface profiling with white-light interference microscopy, Raman spectroscopy, and scanning electron microscopy (SEM). Electrochemical studies, including measuring the potential window, background current and differential capacitance of the prepared electrodes, were performed using 2.5 M H_2SO_4 solution as indifferent electrolyte. The reversibility of the electrode reaction and electroactivity of the electrodes were also studied using the $[Fe(CN)_6]^{3-}/[Fe(CN)_6]^{4-}$ redox system. We further evaluated the durability of the Ti based BDD electrodes under anodic polarization at 2.2 V in 2.5 M H_2SO_4 solution.

2. Experimental

2.1. *Substrate preparation and film deposition*

To provide different degrees of surface roughening, commercially pure Ti (99.6%, ASTM grade 1) plates, of 10 by 18 by 1 mm dimensions, used as the substrates, were annealed by isothermal heating in air at 950 and 800 °C for 2 h, and subsequently air-cooled to form a different grain structure. The surface scale was removed by sand blasting. Details of sandblasting: powder material: SiC, particle size: No. 60 (i.e., 300–250 μm), pressure 3 kgf cm^{-2}, flow rate 142 m^3 min^{-1}.

Thereafter the respective annealed Ti substrates were chemically etched in 6 M HCl at 90 °C to produce a rough surface microrelief. The thickness of the etched plates was somewhat less than 1 mm. We labelled five types of differently treated Ti substrates to be used for diamond deposition from A to E as given in Table 1. The BDD samples deposited thereon are classified according to the Ti substrate type. For comparison, one Ti sample was polished by 3/2 μm diamond paste by leather chamois to a mirror-like surface.

Prior to diamond deposition, the substrates were treated for 15 min in an ultrasonic bath in a slurry of nanodiamond powder (produced by a detonation technique, nominal particle size ca. 5 nm), to provide high diamond nucleation density. The diamond film deposition was performed in a hot-filament CVD reactor. Carburized tungsten wires were heated to 2000 °C to activate the reaction gas (methane gas and methanol vapor, mixed with hydrogen and acetone vapor). The total gas pressure was in the range 30–40 Torr. The carbon content in the mixture varied from 0.5 to 1.1%. The substrate temperature varied in the range 750–950 °C, as measured by an optical pyrometer. For diamond doping by boron, trimethylborate dissolved in methanol was introduced to the reactor during the deposition process. Altogether more than 30 samples of diamond films with thickness from 2 to 5 μm were produced in 5 to 8 h deposition runs. Post-annealing of the as-grown samples was made at 520 to 530 °C in air.

2.2. *Film characterization*

The film structure was characterized using various methods. Raman spectra were obtained with an S3000 Instrument S.A. spectrometer in backscattering mode using Ar^+ ion laser radiation for the Raman scattering excitation. The laser beam at 514.5 or 488 nm wavelengths was focused on a spot 2–5 μm in diameter on the analyzed surface. SEM imaging was performed with a JEOL 6300F microscope. The surface topography, average surface roughness R_a (the average deviation of all points from a plane fit to the test part of the surface) and roughness factor S_{ef} (the true-to-geometrical surface ratio) for bare and diamond-coated Ti were measured on a 180 by 130 μm sampling area with a ZYGO model of White Light Interferometric Microscope (WLIM).

Table 1. Ti substrates used for diamond deposition

Substrate type	Treatment conditions
A	Sandblasted
B	Annealed at 800 °C, sandblasted, etched for 1 h
C	Annealed at 800 °C, sandblasted, etched for 6 h
D	Annealed at 950 °C, sandblasted, etched for 1 h
E	Annealed at 950 °C, sandblasted, etched for 2 h

2.3. *Electrochemical evaluation*

Prior to measurements, the as-grown samples were annealed at 520–530 °C for 20 min in air, to remove any amorphous carbon layer that may have formed on top of diamond during the latest, poorly controlled, stage of the diamond deposition process. Obviously, the diamond films appeared oxygen-terminated upon this treatment.

The electrodes were tested in a three-electrode electrochemical cell. The plane-plate samples were pressed, using an O-ring made of silicon rubber, to the polished rim of an opening in the glass cell wall. The electrode working surface area was ca. 0.2 cm^2. (In what follows, the differential capacitance and current values are given per cm^2 of geometrical surface, unless otherwise specified.) An Ag,AgCl(1 N)-electrode was used as reference; all potentials are given against this electrode. Electrochemical impedance spectra were measured using an R-5021 ac bridge (Russia), in a frequency range 20–200 kHz, or SOLARTRON SI 1280B instrument (Great Britain), 1–20 kHz. The spectra were interpreted using a Randles' equivalent circuit containing a double-layer capacitance (C) and a charge-transfer resistance (R_F) in parallel, with a resistance (R_s) connected in series; elements of the circuit were then calculated by a fitting procedure. Potentiodynamic curves were recorded with linear scanning of electrode potential, using a PI-50-1 potentiostat equipped with a PR-8 programming unit and a PDA-1 x—y recorder (Russia), or the SOLARTRON SI 1280B. The scan rate v varied from 5 to 100 mV s^{-1}.

In preparing the working solutions, we used ultra-high purity H_2SO_4 and analytical grade $K_3Fe(CN)_6$ and $K_4Fe(CN)_6$ chemicals.

The following characteristics were measured:

- potentiodynamic curves recorded in 2.5 M H_2SO_4, in order to estimate the potential window and the background current;
- differential capacitance determined in 2.5 M H_2SO_4 at a steady-state potential (~0.3 V), in order to evaluate the diamond doping level;
- anodic and cathodic potentiodynamic curves recorded in 0.5 M H_2SO_4 + 0.01 M $MK_4Fe(CN)_6$ (resp., $K_3Fe(CN)_6$) at different potential scan rates, in order to evaluate the electrochemical activity of the electrodes.

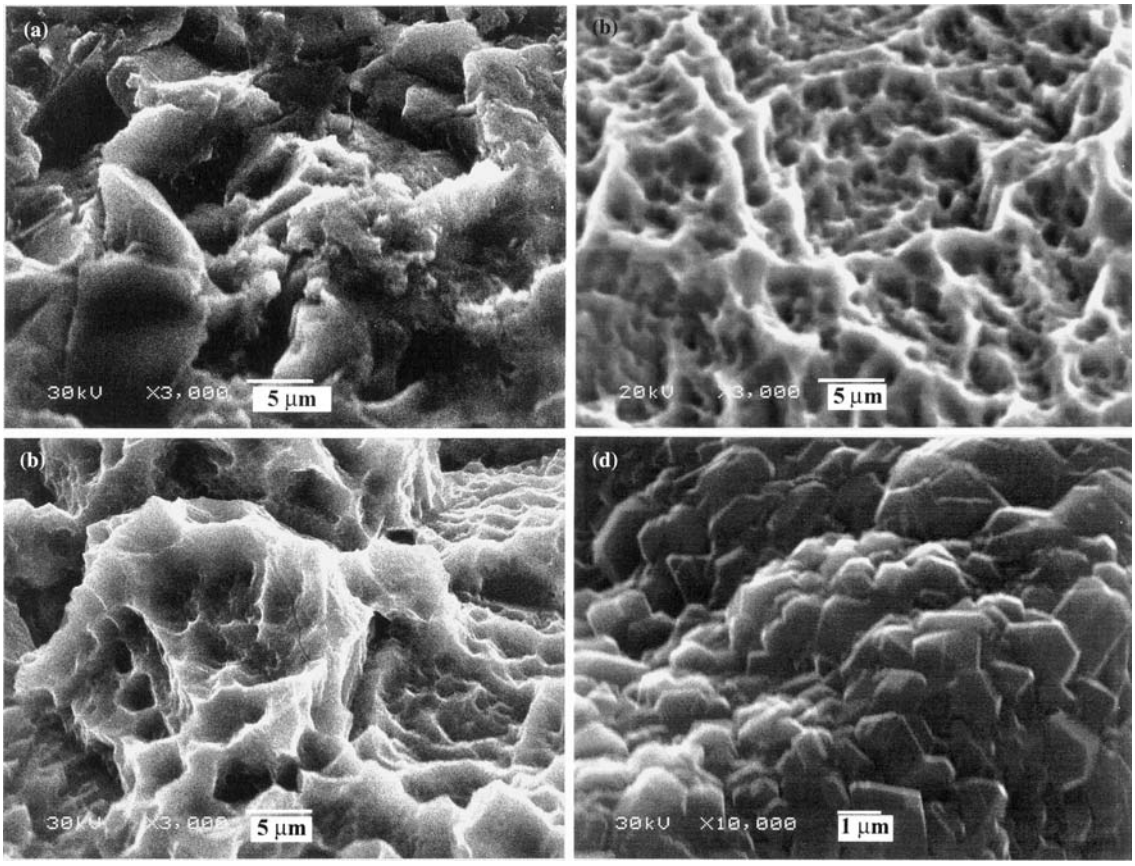

Fig. 1. SEM images of Ti substrate surface for samples A (a), C (b), E (c), and surface of diamond film on sample A (d).

3. Results

3.1. *Surface topography*

The Ti substrates subjected to the pretreatment process provided different degrees of surface roughening (Figure 1a–c). The substrates subjected to etching (types B–E) show more intricate surface as the annealing temperature and/or etching time increased. This observation is corroborated by measurements of surface roughness and effective surface area which show a similar trend. Typically, the diamond films show well faceted crystallites with size in the range from 0.3 to 1 μm (Figure 1d), the grain shape being similar although substrate treatments differed. The surface relief on the macroscale repeated more or less the rough substrate morphology (Figure 2).

The surface roughness R_a and the roughness factor S_{ef} measured prior to and after diamond deposition are listed in Table 2. The roughness R_a increased (up to a factor of six) in the order from A to E as the Ti substrates underwent annealing at higher temperature and/or more prolonged chemical etching. The roughness factor S_{ef} rose to 2.9 for the roughest (type E) substrate. The diamond deposition somewhat reduced the initial roughness and the roughness factor, which might be due to filling of small pits with diamond crystallites. Diamond film on polished Ti shows minimum roughness, $R_a = 0.1$ μm, as might be expected.

It should be noted that the WLIM technique somewhat underestimates the real surface area since the measurement procedure ignores too steep surface features (with slop approaching 90°), and undercut features. However, we believe this does not qualitatively affect the observed tendency in the roughness-treatment relationship.

3.2. *Raman analysis*

The phase purity of the post-annealed diamond films was characterized by Raman spectroscopy which gives a fingerprint of diamond spectra. Representative Raman spectra of selected samples shown in Figure 3 reveal the presence of only a small contribution of amorphous carbon which gives the weak broad peak centered around 1500 cm^{-1}. All samples showed a distinct narrow diamond peak centered in the range 1325–1332 cm^{-1}, indicating that fairly good diamond films are deposited on the Ti substrates. The Raman peak position (1329.0 cm^{-1} as averaged over 23 samples) is systematically shifted toward lower values relative to that for undoped diamond (1332.5 cm^{-1}). This shift, as well as the specific asymmetric peak shape and a broad wing at the lower frequency side (ca. 1230 cm^{-1}) of the diamond peak area, is caused by the Fano effect (interference between discrete zone center phonon and a continuum of electronic excitation) in heavily doped diamond [17]. *Undoped* films on Ti show the diamond peak shifted to

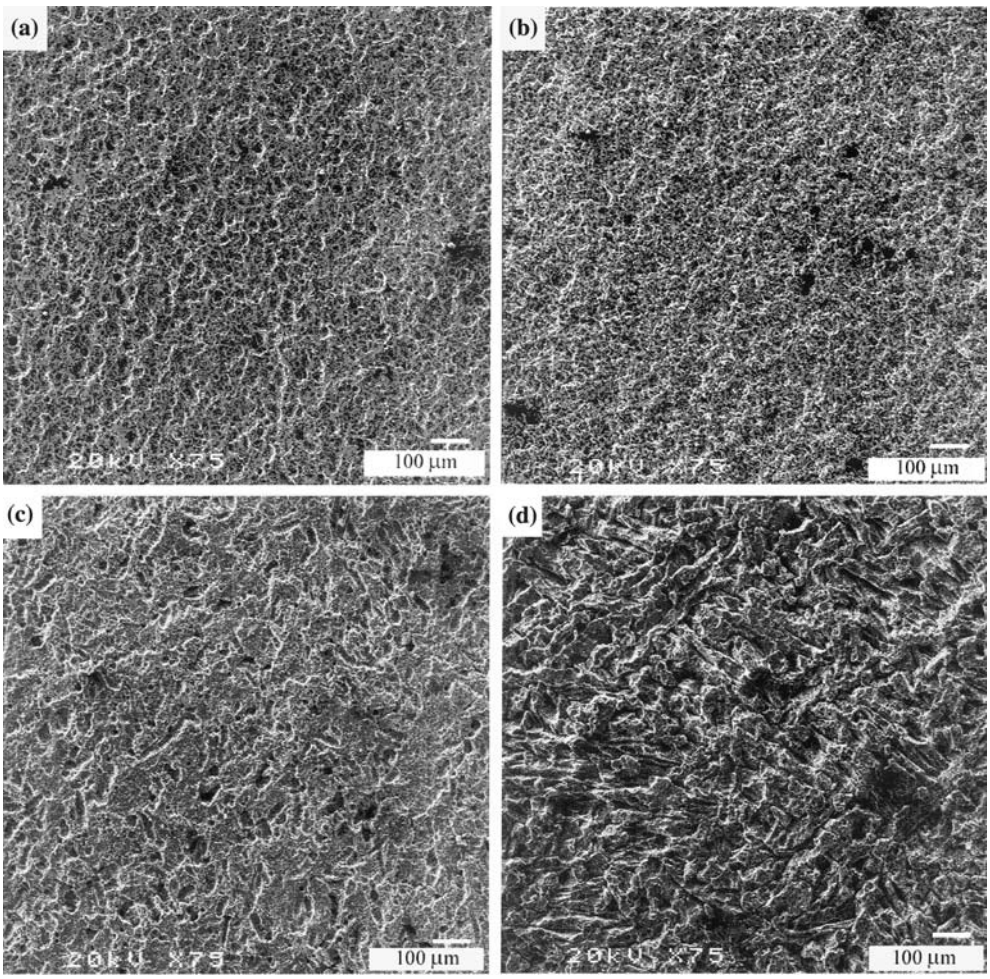

Fig. 2. Low-magnification SEM pictures of the BDD/Ti electrodes of types: (a) B, (b) C, (c) D, (d) E, showing that the diamond films conform to the morphologies of the Ti substrates with different roughness. The scale bar is 100 μm.

Table 2. Surface roughness R_a and roughness factor S_{ef} for pre-treated Ti substrates and diamond-coated Ti electrodes

Ti substrate	Roughness R_a/μm		Roughness factor S_{ef}	
	Before deposition	Diamond-coated	Before deposition	Diamond-coated
Polished	n.a.	0.11	n.a.	1.40
A	1.5	0.36	1.69	1.49
B	2.56	2.48	2.29	2.17
C	3.5	n.a.	2.44	n.a.
D	4.4	3.58	2.64	1.99
E	9.4	n.a.	2.91	n.a

higher frequencies, because of thermal compressive stress generated due to mismatch between thermal expansion coefficients of diamond (0.8×10^{-6} K^{-1} at R.T.) and Ti (8.5×10^{-6} K^{-1} at R.T.). The strong thermal stress, about 7 GPa for the substrate deposition temperature 800 ° C [18], is built-up in the film during the cooling stage after the end of deposition. The Raman peak deviation from the unstressed position at 1332.5 cm^{-1} is proportional to the stress with a gauge factor of -2.05 cm^{-1} GPa^{-1}. However, because of the Fano effect for B-doped films, we cannot determine the stress directly from the Raman peak shift. However, assuming that the thermal stress is negligible because the film thickness is comparable with the characteristic diameter of surface protrusions, from the Raman peak position we estimated [14] the maximal B concentration as $>2\ 10^{20}$ cm^{-3}.

3.3. *Electrochemical studies*

The unetched type A samples were found to differ from all other (etched in HCl) types in having a much higher (2 to 3 times) capacitance: 20.2 μF per 1 cm^2 of geometrical surface on average. Moreover, the etched Ti substrates exhibited (before diamond deposition) the presence of hydrides TiH and/or TiH_2, as detected by

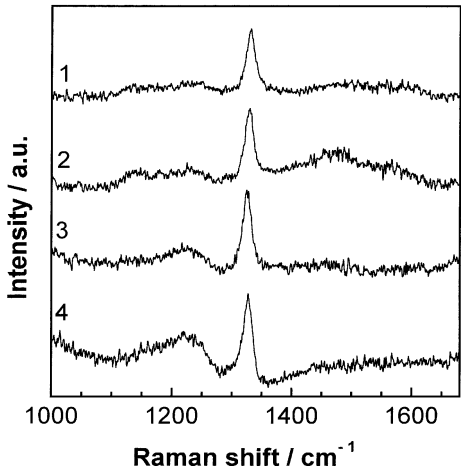

Fig. 3. The Raman spectra of some BDD films deposited on the pre-treated Ti substrates of the E (1), C (2), D (3), and A (4) substrate type. From top to bottom the Fano effect is ever increasing; curve 4 corresponds to the most heavily doped film.

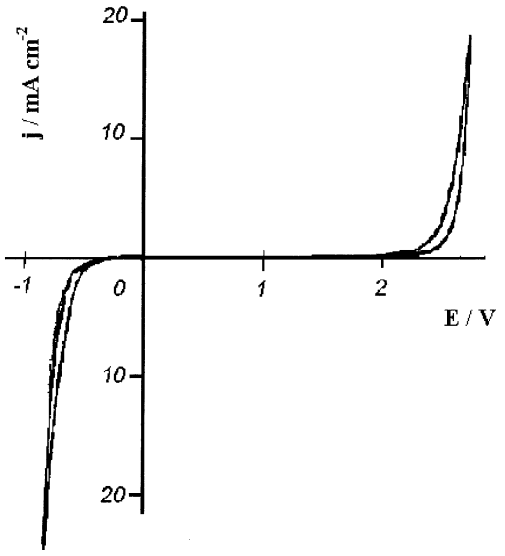

Fig. 4. The determination of the potential window: a cyclic voltammogram (sample on a C substrate) taken in 2.5 M H_2SO_4. The potential scan rate: 5 mV s^{-1}.

X-ray diffraction analysis, while no hydrides, as expected, were found in type A substrates subjected to sandblasting only. As the pre-existing hydride layer should influence the diffusion of H and C in the titanium substrate, this could result in different diamond growth kinetics on the type A substrate. For this reason in what follows we will omit the unetched samples from consideration.

The data obtained are summarized in Table 3. An average of 5 to 7 BDD electrode samples for each substrate type is given, with the RMS deviation in square brackets.

3.3.1. *Potential window*

A typical potentiodynamic curve taken in 2.5 M H_2SO_4 solution is shown in Figure 4. Table 3 shows that the potential window is as wide as ~2.5–2.9 V, which is typical of perfectly crystalline boron-doped diamond films. A very slight trend in potential window is found, the D samples showing the best value of 2.95 V among others.

A minimum positive anodic limit was measured for the high-temperature annealed E samples, which appear to be less suitable anodes for, e.g., electrooxidation of organics species.

3.3.2. *Background current and electrochemical stability*

Typical cyclic voltammograms (taken upon continuous cycling of the electrode potential for 15 min) are shown in Figure 5. In the middle part of the potential window the background current is less than 10 μA cm^{-2}.

To test the long-term electrochemical stability under anodic polarization, we exposed a sample in 2.5 M H_2SO_4 solution at 2.2 V for 40 h. Prior to and upon completing the test, the background current was measured. The background current appeared practically unchanged after the anodic treatment (Figure 5). This suggests high electrochemical stability of the electrodes.

3.3.3. *Differential capacitance*

The measured electrochemical impedance spectra were interpreted using a Randles' equivalent circuit. The bulk resistance of the heavily doped diamond films is much lower than that of the electrolyte and thus cannot be directly measured.

The scattering in the differential capacitance data is rather large (Figure 6), yet some tendency in the variation of the measured values with treatment are evident. Comparing the capacitance of the samples grown on different substrates (see *averaged* values in Table 3), we see that it increases with surface roughness: the group B and C samples have the differential capacitance of ~7 μF cm^{-2}; samples D and E, ~8 and 12 μF cm^{-2} (based on geometrical surface area).

Table 3. Electrochemical parameters of the films

Substrate type	Potential window/V			Transfer coefficients for $Fe(CN)_6^{3-/4-}$ system		Capacitance/μF cm^{-2}	
	Width	From*	To*	α	β	Of true surface	Of geom. surface
B	2.8 [0.25]	−0.5	2.3	0.34 [0.02]	0.37 [0.07]	3.3	6.9 [3.3]
C	2.9 [0.22]	−0.7	2.2	0.37 [0.04]	0.39 [0.14]		7.5 [1.7]
D	2.95 [0.26]	−0.6	2.35	0.38 [0.04]	0.39 [0.03]	4.1	8.3 [1.5]
E	2.5 [0.41]	−0.5	2.0	0.38 [0.08]	0.42 [0.15]		12.6 [3.2]

* vs. Ag,AgCl-electrode.

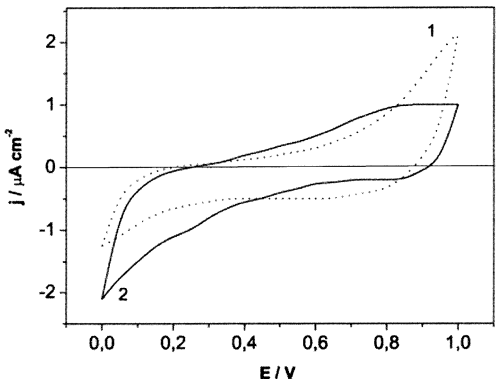

Fig. 5. Effect of the anodic treatment on the background current: cyclic voltammograms in 2.5 M H_2SO_4 (sample on a D substrate) prior to (1) and after (2) a 40 h-exposure to the polarization of 2.2 V. The potential scan rate: 50 mV s^{-1}.

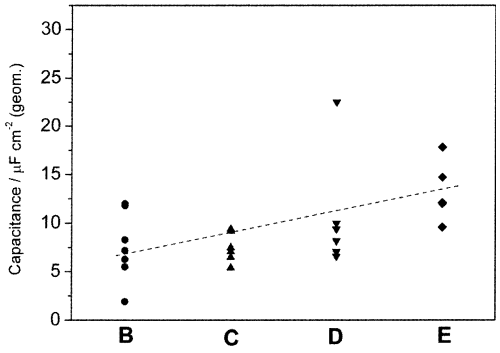

Fig. 6. The differential capacitance for the B, C, D, and E electrodes, demonstrating the surface roughness effect. (All measured values are given, showing the experimental data scatter.)

Allowing for the diamond film surface roughness factor S_{ef} (Table 2), we recalculated the capacitance per cm^2 of true diamond surface as ~3.3 and 4.1 $\mu F\ cm^{-2}$ for B and D samples, respectively.

The differential capacitance values are high for all samples, which is due to both the highly dispersed surface of the electrodes and the high level of diamond doping. Because the semiconductor approach (based on the Schottky theory of space charge) is not applicable to the heavily doped (metal-like) diamond films, we failed in plotting Mott–Schottky lines, unlike the case with moderately doped electrodes [6]. Thus, we can only qualitatively evaluate the doping level from the capacitance value; the acceptor concentration seems to be as high as $10^{21}\ cm^{-3}$ (which agrees with the estimate of $> 2 \times 10^{20}\ cm^{-3}$ given above, section 3.2).

For the great majority of samples, the charge-transfer ("parallel") resistance R_F measured in the supporting electrolyte within the potential window is high (dozens of $k\Omega\ cm^2$, at least). This agrees well with the low background current (less than 10 $\mu A\ cm^{-2}$, as shown in Figure 5) and indicates the practical absence of diamond corrosion or surface side-reactions.

3.3.4. *Electrochemical kinetics*

Typical anodic and cathodic potentiodynamic curves for $Fe(CN)_6^{4-}$ oxidation and $Fe(CN)_6^{3-}$ reduction are given in Figure 7. Both anodic and cathodic curves show current peaks, which indicate a relatively rapid electrochemical reaction in the $[Fe(CN)_6]^{3-}/[Fe(CN)_6]^{4-}$ redox system, so that the rates of the electron transfer stage and of the mass transfer are comparable. The potentials of the anodic and cathodic current peaks E_p depend on the potential scanning rate, v, which points to the irreversible nature of the reaction. From the slope of E_p vs. log v dependencies (Figure 8), we calculated the transfer coefficients for the cathodic (α) and anodic (β) reactions following the kinetic theory [19], using the formula:

$$E_p = \text{const} - 2.3(RT/2\alpha nF)\log v$$

where n is the number of electrons participating in the reaction ($n = 1$), F is the Faraday number, R is the gas constant and T is the absolute temperature. The potential difference between the anodic and cathodic current peaks ΔE_p was also estimated from the voltammograms of the Figure 7 type.

4. Discussion

Concerning the potential window, the background current, and reaction kinetics in the $[Fe(CN)_6]^{3-}/[Fe(CN)_6]^{4-}$ model system, the prepared samples

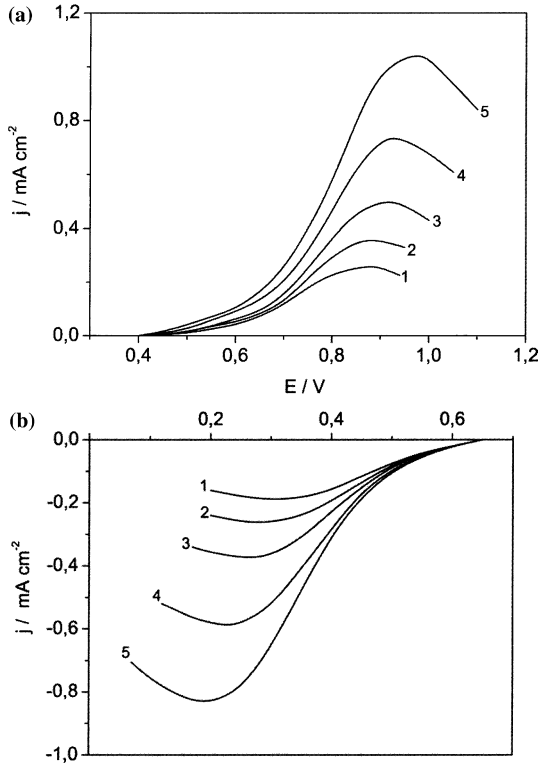

Fig. 7. Anodic (a) and cathodic (b) potentiodynamic curves in the $[Fe(CN)_6]^{3-}/[Fe(CN)_6]^{4-}$ system (sample on a D substrate). The potential scan rate v (in mV s^{-1}): 1–5; 2–10; 3–20; 4–50; and 5–100.

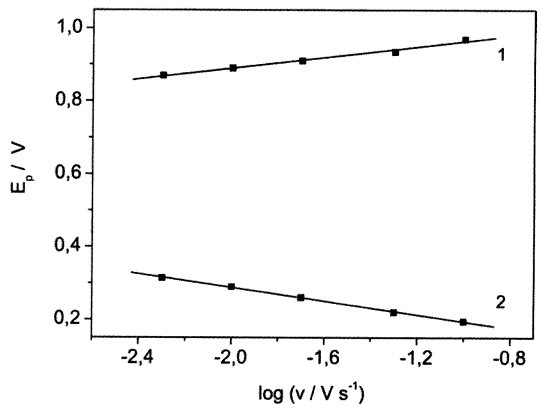

Fig. 8. Determination of the transfer coefficients in the $[Fe(CN)_6]^{3-}$/$[Fe(CN)_6]^{4-}$ system from the dependence of the current peak potential on the logarithm of potential scan rate: 1 – the anodic reaction; 2 – the cathodic reaction (sample on a E substrate).

appeared highly competitive with the best diamond electrodes described in the literature.

The B to E substrates were subjected to annealing, in order to restructure the metal, and to subsequent etching in HCl, which resulted in roughening of the titanium surface. It is the surface roughness factor, that is, the ratio of true-to-geometrical surface area (see Table 2), that has been arbitrarily chosen by us as a characteristic of the substrate surface formed during the pretreatment. Indeed, assuming the same doping level and film quality the only difference between the samples would be in the surface relief. The following discussion is focused on the effects of diamond film surface microroughness on the electrode properties. Some parameters like the transfer coefficient and capacitance showed a clearer dependence on roughness, while others, like the potential window, did not.

4.1. *The potential window*

The B, C, and D electrodes have the widest potential window; however, the variation is rather small, while E electrodes have the narrowest window. Except for E samples, the widening of the potential window may reflect the surface microroughness: the higher the roughness, the lower the true current density.

4.2. *The differential capacitance*

The capacitance increases slightly, but distinctly, from B to E (Figure 6). We speculate that the increase in capacitance is mainly due to the increasing microroughness, rather than the doping level.

4.3. *The electrochemical kinetics*

The current in the $[Fe(CN)_6]^{3-}$/$[Fe(CN)_6]^{4-}$ redox system and its potential dependence suggests that the electrode electrochemical activity is fairly good, despite the diamond surface being oxygen-terminated. According to [20], oxygen-terminated diamond electrodes are less reversible toward the $[Fe(CN)_6]^{3-}$/$[Fe(CN)_6]^{4-}$ system than hydrogen-terminated diamond films. Indeed, the potential difference between the anodic and cathodic current peaks ΔE_p, which can be taken as a criterion of reaction reversibility, even if exceeding the theoretical value of 0.06 V for a reversible electrode reaction, is still rather small, ~0.3 V on average (Table 4; the RMS deviation shown in square brackets).

On analyzing the kinetic data, with due regard for the experimental scatter (Table 3), we speculate that the surface roughness affects the kinetic characteristics of the diamond film electrodes even if slightly. We conclude that the electrochemical redox reaction proceeds in a less irreversible manner on the D electrodes; C and E samples are somewhat inferior to D; still more irreversible are B electrodes. Indeed, the electrochemical activity in the series grows monotonically with roughness: B < C < D ~ E, as evidenced by the increasing $(\alpha+\beta)$ and decreasing ΔE_p values (Table 4). This criterion points to the apparent increase in the reversibility of the electrochemical reaction, which may be explained by the decrease in true kinetic current density in this series, hence, a gradual approach to reversible charge transfer.

The difference in the true surface area does not affect the potentiodynamic curves, Figure 7, because the measured steady-state current is under diffusion, rather than kinetic, control. Indeed, under steady state conditions, the diffusion front has propagated far from the electrode surface, to a distance well exceeding the microroughness size, see, e.g., [21]. Hence, it is the geometrical, rather than the true, electrode surface area that counts. The kinetic parameter ΔE_p is determined by the true current density; hence, it depends on the true surface area. Therefore, roughening of the diamond surface produces no gain in the measured current (e.g., in the electroanalysis); however, the roughening improves the kinetics and carries the reaction from kinetic to diffusion control, thus being beneficial for electroanalytical applications.

Despite their rather high electrochemical reaction reversibility, the E samples are inferior to, e.g., D electrodes: their potential window is narrower; the cathodic current peaks are often lower than the anodic peaks. We may conclude that excessive substrate etching, resulted in the pronounced microroughness,

Table 4. Kinetic parameters of the electrodes

Substrate type	$\alpha+\beta$	$\Delta E_p/V$
B	0.71	0.36 [0.16]
C	0.76	0.30 [0.08]
D	0.77	0.29 [0.16]
E	0.80	0.30 [0.18]

is deleterious to diamond electrode behavior. The reason for this effect still remains an open question.

5. Conclusions

(1) B-doped diamond electrodes on titanium substrates are competitive with the best diamond electrodes described in the literature. The electrodes appear stable in 2.5 M H_2SO_4 solution at high anodic potentials. Studies on their use in electroanalysis of metal ions are in progress. The films appeared rather heavily doped: the acceptor concentration probably being $\sim 10^{21}$ cm^{-3}.

(2) The higher the microroughness, the higher the differential capacitance, while the potential window shows little variation between 2.5 and 2.9 V.

(3) The electrodes demonstrate fast electron transfer in the $[Fe(CN)_6]^{3-}/[Fe(CN)_6]^{4-}$ redox system, the transfer coefficients increasing slightly, and the potential difference between the anodic and cathodic current peaks ΔE_p somewhat decreasing with roughness. Most reversible are D electrodes. The electrochemical activity in the $[Fe(CN)_6]^{3-}/[Fe(CN)_6]^{4-}$ system increases in the order B < C < D $\sim$ E; the electroactivity evidently follows the trend in surface roughness. The apparent increase in the reversibility may be explained by the decrease in the true current density in this series.

Acknowledgments

The authors are grateful to S. Voronina for sample preparation, V. Kononenko for surface profilometry measurements, E. Obraztsova for taking Raman spectra, and S. Chernook for SEM photos. This work was sponsored by the ITRI Innovative and Advanced Technology Research Program (Project A321XS5321) and in part by the NEDO International Joint Research Grant Program (project 01MB9) and the Russian Foundation for Basic Research (project 04-03-32034).

References

1. Yu.V. Pleskov, The Electrochemistry of Diamond, *in* R. Alkire and D. Kolb (Eds.), *Advances in Electrochemical Science and Engineering*, vol. 8, (Wiley-VCH, Weinheim, 2003), p. 209.
2. Yu.V. Pleskov, *The Electrochemistry of Diamond (in Russian)* (Editorial URSS, Moscow, 2003).
3. Yu.V. Pleskov, Yu.E. Evstefeeva, M.D. Krotova, V.V. Elkin, V.M. Mazin, V.Ya. Mishuk, V.P. Varnin and I.G. Teremetskaya, *J. Electroanal. Chem.* **455** (1998) 139.
4. Yu.V. Pleskov, Yu.E. Evstefeeva, M.D. Krotova, V.Ya. Mishuk, V.A. Laptev, Yu.N. Palyanov and Yu.M. Borzdov, *J. Electrochem. Soc.* **149** (2002) E260.
5. T. Kondo, Y. Einaga, B.V. Sarada, T.N. Rao, D.A. Tryk and A. Fujishima, *J. Electrochem. Soc.* **149** (2002) E179.
6. Yu.V. Pleskov, Yu.E. Evstefeeva, M.D. Krotova, V.G. Ralchenko, I.I. Vlasov, E.N. Loubnin and A.V. Khomich, *J. Appl. Electrochem.* **33** (2003) 909.
7. L.C. Hian, K.J. Grehan, R.G. Compton, J.S. Foord and F. Marken, *Diamond and Related Mater.* **12** (2003) 590.
8. Y. Show, M.A. Witek, P. Sonthalia and G.M. Swain, *Chem. Mater.* **15** (2003) 879.
9. K. Honda, T.N. Rao, D.A. Tryk, A. Fujishima, M. Watanabe, K. Yasui and H. Masuda, *J. Electrochem. Soc.* **147** (2000) 659.
10. K. Honda, M. Yoshimura, R. Uchikado, T.N. Rao, D.A. Tryk, A. Fujishima, M. Watanabe, K. Yasui and H. Masuda, *Electrochim. Acta* **47** (2002) 4373.
11. I. Duo, A. Fujishima and C. Comninellis, *Electrochem. Commun.* **5** (2003) 695.
12. T.L. Kulova, Yu.E. Evstefeeva, Yu.V. Pleskov, A.M. Skundin, V.G. Ralchenko, S.B. Korchagina and S.K. Gordeev, *Fiz. Tverd. Tela* **46** (2004) 707.
13. L. Schaefer, M. Fryda, D. Herrmann, I. Troester, W. Haenni and A. Perret, *in* Proceedings of 6th Applied Diamond Conference/2nd Frontier Carbon Technologies Joint Conference (ADC/FCT 2001), Y. Tzeng, K. Miyoshi, M. Yoshikawa, M. Murakawa, Y. Koga, K. Kobashi and G.A.J. Amaratunga (Eds.), NASA/CP-2001-210948 (2001) 158.
14. M. Fryda, T. Matthée, S. Mulcahy, A. Hampel, L. Schaefer and I. Troester, *Diamond and Related Mater.* **12** (2003) 1950.
15. M. Fryda, T. Matthée, L. Schaefer and C.-P. Clages, *Nachr. Chem. Tech. Lab.* **45** (1997) 379.
16. M. Fryda, L. Schaefer and I. Troester, *Recent Res. Devel. Electrochem.* **4** (2001) 85.
17. K. Ushizawa, M. Nishitani-Gamo, C. Xiao, K. Watanabe, Y. Sato and T. Ando, *in* Proceedings of 6th International Symposium on Diamond Materials, The Electrochemical Society, Pennington, USA, **99–32** (2000) 247.
18. J.W. Ager and M.D. Drory, *Phys. Rev. B* **48** (1993) 2601.
19. P. Delahay, *New Instrumental Methods in Electrochemistry* (Interscience Publishers, Inc., New York, 1954)Chap. 6.
20. I. Yagi, H. Notsu, T. Kondo, D.A. Tryk and A. Fujishima, *J. Electroanal. Chem.* **473** (1999) 173.
21. M. Tanaka, K. Aoki, K. Tokuda and H. Matsuda, *J. Electroanal. Chem.* **246** (1988) 1.